Published in final edited form as:
J Neurosci. 2011 March 9; 31(10): 3670–3682. doi:10.1523/JNEUROSCI.4750-10.2011.

Experimental protocols alter phototransduction: the implications for retinal processing at visual threshold

Anthony W. Azevedo and
Department of Physiology and Biophysics, University of Washington

Fred Rieke
Department of Physiology and Biophysics, University of Washington and Howard Hughes Medical Institute

Abstract

Vision in dim light, when photons are scarce, requires reliable signaling of the arrival of single photons. Rod photoreceptors accomplish this task through the use of a G-protein coupled transduction cascade that amplifies the activity of single active rhodopsin molecules. This process is one of the best understood signaling cascades in biology, yet quantitative measurements of the amplitude and kinetics of the rod's response in mice vary by a factor of ~2 across studies. What accounts for these discrepancies? We used several experimental approaches to reconcile differences in published properties of rod responses. First, we used suction electrode recordings from single rods to compare measurements across a range of recording conditions. We next compared measurements of single cell photocurrents to estimates of rod function from *in vitro* electroretinograms. Finally, we assayed the health of the post-receptor retinal tissue in these different conditions. Several salient points emerge from these experiments: (1) recorded responses can be altered dramatically by how the retina is stored; (2) the kinetics of the recovery of responses to bright but not dim flashes are strongly sensitive to the extracellular concentration of magnesium; (3) experimental conditions which produce very different single photon responses measured in single rods produce near identical derived rod responses from the electroretinogram. The dependence of rod responses on experimental conditions will be a key consideration in efforts to extract general principles of G-protein signaling from studies of phototransduction and to relate these signals to downstream mechanisms that facilitate visual sensitivity.

Keywords

rod photoreceptor; Leibowitz L-15; Locke's; Ames; ERG; visual threshold

Introduction

Rod photoreceptors provide the dominant input to the visual system under conditions in which photons are scarce. This requires that rods detect the absorption of single photons and that the resulting signals are effectively read out by the retinal circuitry (reviewed by Sharpe and Stockman, 2000; Field et al., 2005). Our understanding of these processes relies on an accurate description of the rod's responses to single absorbed photons. Yet the amplitude and kinetics of the rod's responses vary by a factor of ~2 across studies (e.g. Calvert et al., 2000; Mendez et al., 2000; Luo and Yau, 2005; Doan et al., 2006; Krispel et al., 2006; Fu et

Corresponding Author: Fred Rieke, Department of Physiology and Biophysics, University of Washington and Howard Hughes Medical Institute, rieke@u.washington.edu, Box 357290, University of Washington, Seattle, Washington 98195, United States.

al., 2008; Doan et al., 2009; Wen et al., 2009; Gross and Burns, 2010; Okawa et al., 2010). These discrepancies hamper attempts to extract general principles of G-protein coupled receptor (GPCR) function from the photoreceptors, and attempts to construct an understanding of rod vision from the molecular to the organismal level. The work described here aimed to understand the origin of these differences.

Studies of single photon responses offer an unprecedented opportunity to understand how activation of single GPCRs leads to the biochemical amplification that is a hallmark of G-protein signaling (Baylor et al., 1979a; Pugh and Lamb, 1993). Activation of rhodopsin leads, through the G-protein transducin and cGMP phosphodiesterase, to a decrease in cGMP concentration, channel closure, and a decrease in current. Recovery of the resulting response depends on inactivation of these components and resynthesis of cGMP by guanylate cyclase. This basic signaling scheme was worked out more than 20 years ago; more recent work has focused on providing quantitative estimates of the relevant rate constants using a combination of biophysical and genetic approaches. Indeed, a large body of work has made rod phototransduction the best understood G-protein cascade in biology (Burns and Arshavsky, 2005; Burns and Pugh, 2010). However, differences in measured rod responses indicate that the resulting quantitative picture depends strongly on recording conditions (Doan et al., 2009; Gross and Burns, 2010).

Here we identify elements of standard recording protocols that alter the measured parameters of phototransduction. We show that conditions for storing the retina can strongly affect rod sensitivity and single photon response kinetics, and can have dramatic consequences for the health of post-receptor retinal tissue. Differences in the extracellular magnesium concentration account for further quantitative differences in the kinetics of recovery from bright light flashes. We attempted to identify *in vitro* conditions replicating those found *in vivo* by recording electroretinograms (ERGs) from isolated tissue. Derived rod responses to both bright and half-saturating flashes were consistent with similar measures from *in vivo* ERG studies. The rod responses derived from the ERG did not, however, exhibit the clear dependence on recording conditions seen in single rod recordings. This discrepancy limits the utility of the ERG in establishing conditions that mimic those found *in vivo*.

Methods

Mice

Female C57BL/6 type mice, 4–6 weeks old, were purchased from either Jackson or Charles River Laboratories. GCAP$^{-/-}$ mice were obtained from Dr. Jeannie Chen. Following 12–14 hours dark adaptation, a mouse was sacrificed and the eyes removed under infrared illumination. The cornea, lens and vitreous were removed from each eye, leaving the retina attached to the retinal pigmented epithelium (RPE) and sclera. This eyecup was placed in a light-tight container in ~50ml of storage solution for use throughout the day (7–10 hrs).

Solutions

The media and their temperatures used in these experiments are the primary variables in this study. Up to three solutions were used in a single experiment: one solution in which to store tissue, another to perfuse the tissue during recording, and a third to fill the recording pipette. Shorthand designations for particular combinations of solutions are defined in Table 1, and all figures maintain the defined color scheme.

Ames' medium (Sigma-Aldrich or Invitrogen) was developed for storage of retinal tissue of rabbits (Ames and Nesbett, 1981). Bicarbonate-buffered Ames' medium (Bicarb. Ames in Table 1) contained 22.6mM sodium bicarbonate, 80K units/l Penicillin and 80mg/l

Streptomycin and was equilibrated with 95%O_2/5%CO_2. Electrodes were filled with HEPES Ames' medium in which sodium bicarbonate was replaced with 15mM NaCl and 10mM HEPES. The pH was adjusted to 7.4 with 1N NaOH, and the osmolality of each medium was adjusted to 280±2mOsm/kg. In some experiments an additional 0.05mM $CaCl_2$ and/or 1.2mM $MgCl_2$ were added to Ames' medium to match the divalent concentrations in Locke's medium.

Leibowitz L-15 culture medium (GIBCO) was supplemented with 10 mM glucose and 0.1 mg/ml BSA (Sigma-Aldrich) and bubbled with 100% O_2. Dissection began at least half an hour thereafter. The light-tight container was placed on ice for cold storage. We did not observe obvious differences in experiments in which the L-15 medium was either prechilled or placed on ice after the dissection. To separate the effects of L-15 and cold storage, we also performed a few experiments with retina stored in warm (32°C) L-15 medium (Table 2).

Locke's medium contained 112.5mM NaCl, 3.6mM KCl, 2.4mM $MgCl_2$, 1.2mM $CaCl_2$, 20mM $NaHCO_3$, 10mM HEPES, 0.02mM EDTA, 3mM Na_2Succinate, 0.5mM Na-L-Glutamate, 10mM Glucose, 0.1mg/ml BSA, 10ml/l BME 100X Vitamins, and 20ml/l 50X BME Amino Acids (Schnapf et al., 1990). The solution was equilibrated with 95%O_2/5%CO_2 and the pH adjusted to 7.4. Electrodes were filled with HEPES Locke's which lacked sodium bicarbonate, amino acids and vitamins and contained 130mM NaCl.

Light Stimuli

Light emitting diodes with peak emission wavelengths of either 465 or 575 nm provided light stimuli. The LED output was attenuated with neutral density filters and focused to a spot by either the microscope objective or the condenser. The LED output was converted to equivalent photons at 501 nm using the measured LED spectrum, calibrated power output and measured rod spectral sensitivity (Baylor et al., 1984). Stimuli were generated by custom software.

Single cell recordings

Suction electrodes were used to record the membrane currents of single rod outer segments (Yau et al., 1977; Doan et al., 2009). Glass micropipettes were pulled to tip inner diameters of ~2μm, then fire-polished to ~1.6μm, coated with butyltrichlorosilane to reduce cell-to-glass adhesion, and the tips were coated in wax to reduce capacitance. Electrodes used for recordings had resistances of 3–4 MΩ. Calomel electrodes and an active bath ground circuit facilitated stable recordings.

Between three and eight times over the course of the experiment day, ~1/12th of a single retina was transferred to a platform of sylgard and finely chopped in a 350μL droplet of storage solution containing 10 units of DNAse (Sigma-Aldrich). The resulting suspension was transferred to a recording chamber on the stage of an inverted microscope equipped with an infrared viewing system. Pieces of retina were allowed to adhere to the bottom of the chamber for five minutes, then perfused (2–3 ml/min, 37 ± 1 °C) for the course of the experiment.

Cells were selected for extended recordings, lasting anywhere from ten to thirty minutes, if their outer segment had not been obviously damaged by the suction procedure and if they had maximal light responses (i.e. dark currents) exceeding 8pA. The dark current and kinetics of the light response were monitored and a recording aborted if these metrics changed noticeably. Dark currents sometimes increased while the kinetics of the response remained unchanged, after which the recording was stable. We attribute this increase in dark

current to an improved electrical seal at the mouth of the electrode. In these cases, responses before the change in dark current were not analyzed.

Single photon responses (response per Rh*) were estimated from the responses to at least 30 flashes at several flash strengths. Responses to a given flash strength were averaged and scaled by the flash strength. Time-to-peak was measured from the beginning of the 10 ms stimulus. Comparing the average responses across flash strengths checked linearity of the responses. We estimated a single photon response using two approaches. First, we scaled the photon density, I (units of photons μm^{-2}), by an average rod collecting area of 0.5 μm^2 (Field and Rieke, 2002) (see Fig. 3G). Second, we extracted the scale factor that produced a best fit between the rising phases (10%-90% of peak) of the mean squared response and the ensemble variance for a collection of responses to a single flash strength, as follows and illustrated in Figure 3G (Baylor and Hodgkin, 1973; Baylor et al., 1979a). The ensemble mean-squared response, μ^2, to a particular flash strength is assumed to be given by $\mu^2 = n^2a^2$, where n is the mean number of Rh* and a is the average single photon response. If the time course of a varies negligibly, the response variance will be dominated by Poisson fluctuations in photon absorption, i.e.,$\sigma^2 = na^2$, where σ^2 is the measured time-dependent ensemble variance. The ratio of the mean-squared response to the variance, μ^2/σ^2, estimates the mean number of Rh* per flash, n. The mean number of Rh* divided by the photon density estimates the collecting area. We performed the scaling procedure for the response ensemble at each flash strength to obtain at least 3 values for n (Figure 3G). The collecting area was estimated from the slope of the best fit line when n was plotted against photon density.

Electroretinograms (ERGs)

Electroretinograms measure the changes in the trans-retinal potential in response to light, reflecting the changes in flow of current across the retina (Fig. 1A–C). To measure electroretinograms of isolated tissue, approximately half of one retina was placed in a custom cylindrical plastic ERG chamber (Fig. 1A). The chamber provided a single electrical pathway across the retina, between a recording electrode at one side and a reference electrode at the other (Fig. 1B). To this end, the cylinder was composed of hollowed-out bottom and top pieces that joined at a ridge around the perimeter. With the top and bottom pieces adjoined, there remained a space between the pieces approximately 300 μm high and 12 mm in diameter to accommodate a flat-mounted piece of retina. Two discs of thin transparent plastic encased the retina, serving to separate solutions in the top and bottom of the ERG chamber. These distinct pools of solution were electrically isolated save through a pair of holes through the transparent discs, each hole 0.7 mm in diameter. For recordings, a circular filter paper was attached through dots of grease to the transparent plastic disc on the top piece of the ERG chamber and a hole punched in the paper in line with the hole in the transparency. One half of one retina was placed ganglion-cell-side-down onto the filter paper, and the bottom and top pieces of the ERG chamber sealed together by a ring of grease around the tissue. The ERG chamber was then placed into the microscope. Recordings with drifting baseline or unstable light responses, likely due to leak of current around the retina, were rejected.

Light stimuli were delivered as described above. The amplitude of the response to a constant stimulus varied across pieces, and depended on the quality of the electrical seal. It was therefore difficult to compare absolute amplitudes of the ERG responses across pieces of tissue, and normalized responses were typically used instead for comparison. Maintaining stable recordings at 36°C was greatly facilitated by perfusion of both sides of the retina. In vitro ERGs had a shape and sensitivity similar to *in vivo* measurements (see Fig. 9; Saszik et al., 2002;Robson et al., 2004;Herrmann et al., 2010), including oscillations during the rising

phase of the b-wave (Fig. 1C) elicited by a 0.2 ms flash (rather than the 10 ms flash used for most experiments).

Derivation of rod responses from ERGs

To derive a rod response from the ERGs, we employed a paired-pulse technique in which the response to a bright, saturating probe flash was measured as a function of a time separation between an initial test flash and the probe flash (Fig. 1D) (Lyubarsky and Pugh, 1996;Pepperberg et al., 1997;Hetling and Pepperberg, 1999). The derivation of a rod response involved comparing the response to a probe flash that followed a test flash with the response to the probe flash alone (Fig. 1D, E). Responses to the probe flash were isolated by subtracting the response to the test flash alone. The amplitude of the resulting responses was measured at the time of the a-wave's maximum rate of change in response to the probe alone, typically ~15ms (Fig. 1E). The probe flash strength and measurement during the rising edge of the resulting response was used primarily to avoid bleaching the rod photopigment with probe flashes sufficiently bright to produce an a-wave that peaked at less than 15 ms. Some recording conditions also produced dramatic alterations in the ERG b-wave, which could mask or reveal differing amounts of the a-wave; measuring the probe response during its leading edge minimized sensitivity to such alterations of the b-wave. Elimination or disruption of the b-wave occurred either pharmacologically following addition of 4mM aspartate to the perfusion (Fig. 1D–E) (Green and Kapousta-Bruneau, 1999) or as a result of the experiment media (see Fig. 8).

The two parameters of importance in the paired-pulse protocol are the strength of the test flash and the delay between the test and probe flashes. The probe flash strength is constant and is sufficiently bright to saturate the rod response and hence determine the dark current remaining at the time of the probe flash. The remaining dark current depends on the strength of the test flash and the delay between test and probe flashes. In one extreme, the test flash saturates the rods and the presentation of the probe flash during this saturation produces no subsequent response. In the other extreme, the time between test and probe flashes is sufficient to allow the rods to recover fully, and the response to the probe flash is identical to that when the probe flash is presented alone. Cones are not expected to contribute substantially to the ERG a-wave (Lyubarsky and Pugh, 1996); consistent with this expectation, ERGs from transducin knock-out mice ($GNAT1^{-/-}$) (Calvert et al., 2000) recorded in Ames' medium did not exhibit noticeable a-waves over the range of flash strengths used here (data not shown).

The ratio of the probe responses at each time delay t_i to the response to the probe alone estimates the fraction of remaining rod circulating current as a function of time, $R(t_i)$. We then define:

$$F(t_i)=1-R(t_i)$$

where $F(t_i)$ gives the derived rod response. For bright test flashes that saturate the rod circulating current, we fit $F(t_i)$ with the following model of the recovery phase:

$$F'(t)=\frac{1}{(1+e^{a(t-t_{1/2})})^{h}}$$

where $t>0$ is time, and a, $t_{1/2}$, and h are constants. We used this model to interpolate between the measured points and estimate the time required, T_{sat}, for the responses to recover to a criterion level of 0.5. We repeated this procedure for three flash strengths and estimated the

dominant time constant for decay of light-activated PDE activity from the slope of the relation between T_{sat} and the logarithm of the flash strength.

We used different recovery criteria to determine dominant time constants for single cell (criterion of 0.15; Krispel et al., 2006; Burns and Pugh, 2009; Doan et al., 2009) and ERG recordings (criterion of 0.5; Lyubarsky and Pugh, 1996; Hetling and Pepperberg, 1999; see Fig. 6). The low criterion in the case of single rods minimizes sensitivity to the trajectory of the response recovery by 'catching' the response soon after recovery begins. Because the ERG reflects activity of many rods, however, a similar low criterion would bias the dominant time constant towards those rods that recover most quickly. Instead, the criterion of 0.5 should better capture the average response. Consistent with this, the dominant time constant for the ERG-derived responses depended on the criterion that defined recovery, with lower criteria producing faster dominant time constants. Importantly, lower criteria produced faster dominant time constants in all recording conditions, and the similarity of the dominant time constant across recording conditions remained for criteria between 0.1 and 0.5 ($p > 0.24$, Mann-Whitney-Wilcoxon rank-sum tests, comparison of τ_D between Ames'/Ames' and Ames'^{Ca,Mg}/Ames'^{Ca,Mg}). Further, the differences between ERG-derived and single cell recovery kinetics exceed those reported if similar criteria (0.15 or 0.5) are used to measure time in saturation for both types of data.

We also applied the paired-pulse technique to test flashes that produced approximately half-saturating responses (~30 Rh*). We fit the normalized derived rod response with the model from Hetling and Pepperberg (Hetling and Pepperberg, 1999):

$$F'(t)=\gamma[1-e^{-\alpha(t-t_d)^2}]\cdot e^{-t/\tau_\omega}, \quad t>t_d$$

where for $t<t_d$, $F'(t) = 0$. Derived responses with and without 4mM aspartate added to the perfusion solution were similar and hence the measurements were combined.

Experiments were designed such that the cumulative light exposure during a typical recording bleached <3% of the total rod photopigment; furthermore, the retina was allowed to recover for >25sec between test flashes. Data was rejected if responses to periodically-delivered probe flashes exhibited systematic changes indicative of long term adaptation.

A concern about this approach is that bright test flashes could alter the kinetics of the probe response and hence bias the derived responses. Two observations indicated such effects were minimal. First, the impact of changes in the kinetics of the probe response would be expected to depend on probe flash strength - with smaller effects for brighter probe flashes which more quickly saturate the rods. However, derived responses to probe flashes ranging from 840 Rh*/rod to 9900 Rh*/rod were similar ($R^2 = 0.06$, $p = 0.5$, $n = 9$). Similarly, changes in the kinetics of the probe response could cause the derived measurements to depend on the rising phase time-point where we compared probe responses. However, derived rod responses (e.g. Figures 6 and 7) did not systematically depend on the time at which we measured the probe response ($R^2 = 0.01$, $p = 0.15$, $n = 175$, for all points ~12ms-20ms in Ames'/Ames' control conditions, ~12ms-40ms in Ames'/Ames' with 4mM Aspartate, Fig 1E). As a further check, we performed identical experiments on individual rods, which should show similar sensitivity to changes in probe flash kinetics. Dominant time constants measured using the paired-flash approach and measured directly from the test flash response did not differ noticeably (see Fig. 6D–E).

Data collection and analysis

Recorded responses were filtered at 30Hz or at 300Hz (8-pole Bessel) and digitized at 1kHz by an ITC16 or ITC18 A-to-D converter (HEKA). Digitized responses were collected and stored using custom recording software written in C and Igor. Single cell data were digitally filtered at 15Hz, while ERG data were low-pass filtered at 100Hz and the 60Hz sine wave that best fit baseline noise was subtracted, unless otherwise noted. Data was organized using custom software (Phyzion Consulting) and further analyzed using custom Matlab routines (Mathworks).

Live/Dead Staining Assay

To test the effects of tissue storage solutions on the viability of the retina, we imaged retinal cell body layers following staining with a mammalian Live/Dead Cell assay kit (Invitrogen). The protocol assays the integrity of the cell membrane by staining with calcein AM and ethidium homo-dimer1 (EthD-1). If the membrane is intact, the cell retains esterase function capable of hydrolyzing the AM group, and cells will retain the calcein dye in their cytosol. If the membrane is compromised, EthD-1 can access the nucleus and stain DNA. Before staining, 4 μM EthD-1 and 2 μM calcein AM dyes were added to 10ml of Ames' medium. Approximately one third of a retina was placed in the staining solution for 30 minutes before adhering the tissue to filter paper (Anodisc, Whatman), securing the filter paper to the bottom of a recording chamber with vacuum grease and placing the mounted tissue in the microscope. The mounted retina was then always perfused with Ames solution at room temperature (~24 °C). Confocal image z-stacks were taken through the layers of cell bodies with a Nikon laser scanning confocal microscope system using lasers with peak wavelengths of 488 nm to excite the calcein dye and 543 nm to excite the EthD-1 homodimer. Image analysis was carried out in ImageJ. The pixel intensity in each channel was adjusted post-hoc to linearly span the entire range of pixel intensities. Membrane integrity, and cell health, was assessed by the appearance of EthD-1 staining in the nucleus. The cells visibly stained in the EthD-1 channel in ganglion cell layers were counted by hand using the ImageJ Cell Counter plugin.

Statistics

All values reported in the text are given as mean ± standard error of the mean (SEM). Significance was tested using Mann-Whitney-Wilcoxon rank-sum tests (MWW test).

Results

Differences in the reported properties of the single photon responses of mouse rods are strongly correlated with differences in experimental protocols - specifically the solutions used to store and perfuse the retina. We start by determining how the responses of single rod photoreceptors depend on recording conditions. We then measure the effect of recording conditions on estimates of rod function derived from the electroretinogram, and compare those measures to the single cell data. Finally we compare the physiological and morphological viability of the retina under these different conditions.

Experimental conditions alter the kinetics and amplitude of responses of single rods

We recorded the light responses of single rod photoreceptors in several experimental conditions (Table 1; Fig. 2). Commonly used protocols include storing the retina in Leibowitz L-15 culture media and recording in Locke's solution (L-15/Locke's, Table 1; e.g. Baylor et al., 1984;Xu et al., 1997;Makino et al., 2004;Krispel et al., 2006) or storing and recording in Ames' solution (Ames'/Ames', Table 1) (e.g. Field and Rieke, 2002;Doan et al., 2009;Okawa et al., 2010). Consistent with previous results, these protocols produced

substantial differences in the kinetics and sensitivity of the rod responses (Table 2; Fig. 2A–C).

Differences in rod sensitivity could be due either to differences in the ability to capture incident photons and produce an electrical response, or to differences in the amplification of the signal produced by rhodopsin activation. To test for differences in effective photon capture, we used a frequency of seeing analysis (Baylor et al., 1979a) applied to responses of GCAP$^{-/-}$ mice (Mendez et al., 2001; Burns et al., 2002). These rods produce larger and more distinct single photon responses than wild-type rods because of the lack of Ca^{2+}-feedback control of cGMP synthesis (Fig. 3A, D) This allowed accurate determination of the fraction of presentations of a fixed-strength flash resulting in a response (effective absorption of one or more photons) or failure (no effective photon absorptions) (Fig. 3B, E). The failure probability from Poisson statistics is $p_0(I) = e^{-mI}$, where I is the photon density (photons μm^{-2}), and m is the collecting area of the rod in units of μm^2. Figure 3C plots the response probability ($1-p_0(I)$) against flash strength for GCAP$^{-/-}$ rods in L15/Locke's (red) and Ames'/Ames' (black); smooth fits assume Poisson statistics. Estimated collecting areas were not different (Fig. 3F, 0.50 ± 0.04μm^2, mean ± SEM, n = 5, vs 0.47 ± 0.02μm^2, n = 8, p = 0.52, MWW test).

Collecting areas are often estimated by comparing the time-dependent variance of the responses to a repeated dim flash with the square of the mean response. Assuming that the time-dependent variance is dominated by Poisson fluctuations in photon absorption, the ratio of the square of the mean response to the variance provides an estimate of the mean number of effective rhodopsin activations, n, produced by the flash. We used the initial part of the square of response to compute n to avoid variability in the falling phase of the response which could systematically bias the estimate. We applied this procedure to ensembles of responses to increasing flash strengths from wild-type rods in the L15/Locke's and Ames'/Ames' conditions (Fig. 3G, example cell in Ames'/Ames'). The thick traces in Figure 3G compare the scaled ensemble mean-squared response with the ensemble variance (thin traces) for three flash strengths. The collecting area, m, was determined from the slope of the n vs. I data (Fig. 3G, main panel), where I is the flash strength in photons μm^{-2}. We then divided the mean response to each flash by $n' = m\,I$, the flash strength in terms of Rh*, to arrive at an estimate of the single photon response. Finally we averaged these estimates across flash strengths.

Figures 3H and I show, for each cell, the area (charge) under the single photon response derived from the variance analysis plotted against that derived using a fixed collecting area. For the Ames'/Ames' condition (Fig. 3H), single photon responses estimated from variance analysis do not differ systematically from those estimated using a fixed collecting area, likely because variability of the initial ~200 ms of the response is dominated by Poisson fluctuations (Doan et al., 2009). For the L15/Locke's condition, estimates of the single photon response using variance analysis are consistently larger than those using the fixed collecting area (Fig. 3I). This larger single photon response likely results because the assumed dominance of Poisson variation of rhodopsin activation does not hold, and variation in the response to a single Rh* contributes to the time dependent variance (see Methods). The results of Figure 3 raise a general note of caution about the use of variance analysis - i.e. that any manipulations of phototransduction that alter response variability could produce artifactual changes in the collecting area, resulting in errors in estimating the number of activated rhodopsin molecules and the single photon response.

The similarity of the collecting areas determined by the frequency of seeing analysis in GCAP$^{-/-}$ mice suggests that the differences in sensitivity in L15/Locke's and Ames'/Ames' are due to differences in the single photon response. We estimated the average responses of

mouse rods to activation of single rhodopsin molecules under an array of conditions assuming a collecting area of 0.5 μm^2. Single photon responses using the L15/Locke's condition were smaller and faster than those in Ames'/Ames' (Fig. 4A and B, Table 2). Both factors contribute to the reduced sensitivity (Baylor et al., 1979b).

Do the differences in kinetics and sensitivity of the L15/Locke's and Ames'/Ames' conditions reflect differences in retina storage or recording solutions? To answer this question we used warm Locke's medium for both storage and recording. The stimulus-response relation for the Locke's/Locke's condition fell between the red and black curves in Figure 2C (Table 1). The estimated single photon response also showed intermediate amplitude and kinetics (Fig. 5A, B, blue curves), indicating that measured responses were sensitive to both storage and recording conditions. We separated the effects of temperature and L-15 storage by measuring dim flash responses in rods stored in warm L-15 medium (Table 2). In these rods, kinetics and dim flash response amplitude fell between those of rods from retina stored in cold L-15 and Locke's solution, suggesting that both the cold and the L-15 contribute to changes in kinetics.

The remaining differences between the Locke's/Locke's and Ames'/Ames' conditions appeared due to differences in divalent concentrations, as responses measured in Ames' and Locke's media with matched Ca^{2+} and Mg^{2+} concentrations were not distinguishable (Fig. 5A, B, green curve, Table 2). Mg^{2+} differs more substantially between Locke's and Ames', and Ames' medium with elevated Mg^{2+} alone also produced fractional responses and kinetics indistinguishable from those in Locke's/Locke's, though dark currents were reduced (Fig. 5A, B, magenta curve, Table 2).

The dominant time constant of recovery depends on extracellular magnesium

Differences in the time course of the single photon responses in Ames'/Ames' and L15/Locke's (Fig. 4) could reflect differences in cGMP hydrolysis or synthesis or both. The kinetics of the decay of light-activated PDE activity can be monitored from the recovery from bright, saturating flashes (Pepperberg et al., 1992). Recovery of the circulating current following a bright flash requires that the rate of synthesis of cGMP exceeds the rate of hydrolysis by PDE. Under the assumptions, 1) that cyclase synthesis rate is constant while the rod remains saturated, and 2) that PDE deactivation follows an exponential decay, the time at which the rod current begins to recover, T_{sat}, should scale linearly with the logarithm of the flash strength (Fig. 5C, D). The slope of this initially (< 1000 Rh*) linear relationship between T_{sat} and the logarithm of the flash strength (best fit line in Fig. 5D) is the time constant of the assumed exponential decay of PDE hydrolysis and is often termed the dominant time constant of recovery, τ_d.

Figure 5E and F collect measurements of the dominant time constant across conditions. The dominant time constants for rods recorded in L-15/Locke's are consistent with previously reported values (Fig. 5E, F and Table 2) (e.g. Chen et al., 2000; Calvert et al., 2001; Makino et al., 2004; Krispel et al., 2006; Gross and Burns, 2010). The dominant time constants for the Ames'/Ames' condition were significantly longer, again consistent with past work (Doan et al., 2009; Gross and Burns, 2010). Dominant time constants for the remaining conditions (Locke's/Locke's and Ames' with elevated divalents) were all significantly faster than the Ames'/Ames' condition, and closer to the L-15/Locke's condition (Fig. 5F and Table 2). Thus, changes in Mg^{2+} and Ca^{2+} can significantly affect the dominant time constant and account for differences in dominant time constant across recording conditions.

The dependence of the dominant time constant for the decay of light-activated PDE activity on divalent concentrations is striking given the relatively small changes in the single photon responses. In the L-15/Locke's condition, the time constant for the decay of the dim flash

response and the dominant time constant are similar. Such a similarity is expected if the rate of cGMP synthesis is sufficiently rapid that the cGMP concentration closely tracks the PDE activity, and hence the recovery of the dim flash response is limited by the rate of decay of PDE activity. Such rapid cGMP synthesis, however, appears not to always be the case; specifically, in Ames' with elevated divalents the cGMP concentration following a dim flash appears to recover to its dark value slowly compared to the decay of light-activated PDE activity.

Dominant time constants derived from the ERG are similar across experimental conditions

Rod responses *in vivo* are often assayed using the electroretinogram (ERG). To determine if we could use the ERG to identify *in vitro* conditions that closely replicate the *in vivo* rod responses, we derived rod responses from *in vitro* ERGs under a variety of conditions. We compared the derived rod responses to the single cell data summarized above and to properties of *in vivo* ERGs.

We used a paired-flash approach to derive the time course of the rod response from the ERG (Lyubarsky and Pugh, 1996). In this approach, the response to a "test" flash is probed using a second, bright "probe" flash (Methods). We then compare the a-wave, the leading edge of the ERG, in response to the probe flash either alone or following the test flash. We describe the other components of the ERG below; these differed substantially across recording conditions.

We carried out the paired-flash analysis using two types of test flashes: bright flashes producing >200 Rh*/rod, and "dim" flashes producing ~30 Rh*/rod. Previous paired-flash studies using comparable flash strengths show that rod responses derived from *in vivo* ERGs recover quickly following bright flashes (dominant time constant of 140–200 ms, (Lyubarsky and Pugh, 1996; Hetling and Pepperberg, 1999) and dim flashes (time-to-peak of 86 ms, decay time constant 163 ms (Hetling and Pepperberg, 1999)). The relatively fast kinetics of *in vivo* ERG-derived responses, and their resemblance to the kinetics of single cell currents in L-15/Locke's (Table 2), support the conclusion that L-15/Locke's responses are physiologically accurate (Burns and Pugh, 2010). This conclusion relies on the sensitivity of the rod responses derived from the ERG to alterations in the rod transduction currents.

We focused on comparing derived rod responses for conditions that produced pronounced differences in the responses of single rods. In the bright flash regime we compared the derived dominant time constant for recovery in Ames' with that in Ames' with elevated divalent concentrations; these conditions produced dominant time constants in single rods that differed by a factor of ~2 (380 ms vs 170 ms, Table 2). Figure 6A superimposes raw traces from such an experiment. The response to the probe pulse (second flash, ~830 Rh*/rod) reflects the extent to which the rods have recovered following the test flash (~830 Rh*/rod). Responses were aligned to the time of the probe flash and corrected by the amplitude at that point (Fig. 6B). Values of $R(t_i)$ were evaluated at the point of maximum rate of change (~16ms) of the response to the probe flash alone (thick black trace). Figure 6C plots response suppression ($1-R(t_i)$) as a function of the delay between test and probe flashes. The gray line is an empirical fit (see Methods) to the recovery used to interpolate between the measured points.

Two control experiments indicated that the derived responses were dominated by the rods. First, adding 4mM aspartate to the perfusion solution to eliminate responses produced downstream of the rods did not significantly change the results. Second, in retinas from transducin knockout mice (Calvert et al., 2000), bright flashes (>1000 Rh*/rod) produced

ERGs ~100 times smaller than those of wild-type mice (data not shown), indicating that mouse cones make a negligible contribution to the a-wave at these flash intensities.

We repeated the procedure of Figure 6A–C for at least three test flash strengths and used the resulting measures of T_{sat} (Fig. 6D inset) to determine the dominant time constant τ_d. In the standard Ames' condition (Ames'/Ames'), τ_d of the ERG-derived rod response was 200±15 ms (mean ± SEM, n= 9, Fig. 6G); this is within the range of *in vivo* ERG measurements, but is substantially different ($p<0.001$, MWW test) than the average dominant time constant measured from single rods (376 ± 23 ms; Fig. 5F). Increasing the divalent concentration in Ames did not change τ_d (green column in Fig. 6G, n=5, p=1 MWW test). Thus the ~2-fold change in τ_d of the single rod responses is not reflected in the ERG-derived rod responses.

Could the differences in τ_d measured using paired-flash ERGs and single cell recordings reflect differences in experimental protocol? To check this, we measured τ_d from single rod outer segments using both saturation time following single bright flashes (as in Fig. 5) and paired-pulse experiments in the same cell (Fig. 6E–G, Ames'/Ames', n=12). The two approaches provided indistinguishable ($p = 0.9$, MWW test) and highly correlated measures of τ_d (connected points in Fig. 6G; $r=0.94$). In both cases the average τ_d exceeded that derived from the ERG ($p<0.005$ for both methods, MWW test). The average τ_d of single rods using the paired-pulse approach does not differ significantly from the population of rods in Figure 5 ($p=0.6$, MWW test), indicating that the paired-pulse approach probes the rod response as expected.

Kinetics of ERG-derived half-saturating responses in Ames' are consistent with *in vivo* measurements

We also used the paired-pulse approach to derive the time course of the rod response to a sub-saturating flash (Fig. 7). The test flash (~30 Rh*) used in these experiments suppressed, at peak, about half of the response to the probe flash, reflecting a compromise between delivering few photons and eliciting a response large enough to produce measurable current suppression. This test flash is approximately equal to that used in previous ERG measurements (Hetling and Pepperberg, 1999).

In comparing rod outer segment current responses to ERG-derived estimates, it is important to note that in single rods, half-saturating current responses differ in kinetics substantially from single photon responses (Fig. 7A and B, Table 2) (Sampath et al., 2005; Burns and Pugh, 2010). Furthermore, differences across solutions are not as large when comparing half-saturating responses: i.e. the range of values for the time-to-peak across recording conditions is larger for single-photon responses (Fig. 7A, x-axis), than for half-saturating responses (y-axis). Nonetheless, the half-saturating response measured in L-15/Locke's still reaches peak earlier than in Ames' (Table 2, Fig. 7B). Consequently, we compared ERG-derived half-saturating responses in L-15/Locke's and Ames'/Ames' conditions. As in the bright flash regime, we measured the suppression of the probe response for a range of delays between test and probe flashes (Fig. 7C and D lower panel). We averaged the responses at each time point across retinae for each condition and fit the population average with a model for *in vivo* ERG-derived responses (Hetling and Pepperberg, 1999) (Fig. 7E, thin traces). The addition of 4mM aspartate to the perfusion media did not systematically affect the parameters of the fit, so measurements obtained in the absence and presence of aspartate are combined. The derived rod response in L-15/Locke's closely tracks that in Ames'/Ames', with peaks at 82 ms and 76 ms respectively, and with recovery time constants of 191 ms in L-15/Locke's and 139 ms in Ames'/Ames'. For comparison, the grey stippled line shows the best fit model from the Hetling and Pepperberg *in vivo* ERG recordings (Hetling and Pepperberg, 1999) with a time-to-peak of 87 ms and recovery time constant of 163 ms.

Thus, derived rod responses in Ames'/Ames' and L15/Locke's are not readily distinguished, and both are consistent with *in vivo* measurements.

Experimental conditions alter retinal morphology, health, and physiology

The results of the paired-pulse analysis indicate that storage and perfusion solutions do not significantly affect ERG-derived rod responses. We were also interested in how well different experimental conditions maintained post-rod retinal processing, permitting rod responses to be tracked through retinal circuits. We found profound differences in the responses and health of the post-rod circuitry under different experimental conditions.

We recorded electroretinograms of isolated retina to judge overall retinal physiology under different conditions. We subjected each eye to a different protocol and always recorded last from tissue from the Ames'/Ames' condition to ensure that abnormal responses were not due to prolonged storage. Normalized average responses to flash families recorded using L-15/Locke's (Fig. 8A) were highly variable, whether compared to tissue from the same mouse stored in Ames' (matched panels in Fig. 8C), or to other tissue samples treated with L-15/Locke's. The traces in Figure 8A are the averages of 4–6 responses; each individual response is of a stereotyped form (bottom panel, Fig. 8A), indicating that the abnormal form of the ERG does not change during recording. The responses in the middle column (Fig. 8B) come from retinas treated with the various "intermediate" conditions and largely resemble responses in the Ames'/Ames' condition. Comparisons of responses from the L-15/Locke's and Locke's/Locke's conditions (Fig. 8B, blue traces) indicate that L-15 cold storage in particular is responsible for the response variability.

We further assessed the state of retinal tissue by observing tissue morphology in the ganglion cell layer in flat-mounted preparations. Most (>95%) of the ganglion cells in flat-mounted pieces of retina stored in Ames' appeared healthy (Fig. 8F) and produced robust changes in the rate of action potential generation in response to light (not shown). After storage in cold L-15 (Fig. 8D) the morphology of the retinal ganglion cells was abnormal: nuclei appeared bloated and distinct (white arrow), and the retina lacked a smooth quality that accompanies typically healthy and responsive tissue (circles). In addition, attempts to record light responses failed because the cell membranes were too fragile to seal onto with a patch electrode. Ganglion cells in tissue stored in warm Locke's solution (Fig. 8E) lacked the dramatically abnormal appearance of tissue stored in cold L-15, and approximately half of the cells were intact and suitable for recording. The distinct differences in ganglion cell health caused us not to pursue experiments to compare the impact of altered solutions on retinal output.

To better assess the state of the tissue in each condition, we used a cell staining assay that discriminates between living and dead cells based on the integrity of the cell membrane (Methods). Figures 4G–I show confocal images of the ganglion cell layer, where live cells are labelled with calcein-AM (blue) and dead cells with EthD-1 (yellow). Retina from the Ames'/Ames' condition was imaged after retina stored in L-15, and hence served as a control for the effects of storage duration. Cold storage in L-15 results in more yellow-stained cells than any of the other storage conditions: L-15 - 119 ± 32 (n = 8); Locke's - 5 ± 1.7 (n = 4); Ames'^{Mg} - 2 (n = 2); Ames' - 2.6 ± 0.9 (n = 5). L-15 storage produced noticeable, but less dramatic, differences in the bipolar cells in both differential-interference contrast and live/dead cell images (data not shown). Rod bipolar light responses from retina stored in L-15 were highly variable, and thus we did not attempt to compare them with those from retina stored in Ames' medium. Retinas imaged following warm L-15 storage also had extensive yellow staining (130 ± 40 cells, n = 3). Thus L-15 storage compromises retinal health and is not ideal for studies of responses downstream of the photoreceptors.

As a test for more subtle variations in retinal processing, we compared complete ERG waveforms across conditions with properties of *in vivo* ERGs. Average flash responses exhibit a form resembling the *in vivo* ERG response over the scotopic range (Saszik et al., 2002), showing what appeared to be a scotopic threshold response and developing both an a-wave and a b-wave as the flash strength increases (Fig. 9A). The normalized b-wave amplitudes (from baseline) show similar sensitivity across conditions, reaching a half-maximal response near 3 Rh*/rod (Fig. 9B); this is close to the half-maximal flash strength measured directly from rod bipolar cells (Field and Rieke, 2002). Accounting for the optics of the eye (Gross and Burns, 2010; Herrmann et al., 2010), 3 Rh*/rod corresponds to approximately 0.006 cd s/m^2, similar to the half-maximal flash strength of 0.003 cd s/m^2 measured *in vivo* (Herrmann et al., 2010). The time-to-peak of the ERG b-wave in Ames' medium (black curve) ranged from 102 ms to 114 ms over the light intensities in Figure 8 (Fig. 9C), comparable to *in vivo* measurements of 110 ms over the scotopic range (Saszik et al., 2002); the time-to-peak was insensitive to changes in divalent concentration. The b-wave measured in Locke's medium was significantly slower across flash intensities ($p<0.1e-10$, MWW test, all b-wave time-to-peak values in Ames'/Ames' vs. Locke's/Locke's). This may be a result of altered synaptic processing due to the presence of HEPES in Locke's solution (Hirasawa and Kaneko, 2003; Davenport et al., 2008; Fahrenfort et al., 2009).

Discussion

The substantial differences between measured properties of single photon responses across studies hinder progress in two broad areas. First, rod phototransduction is the best-studied example of how G-protein signaling cascades amplify activity of single active receptors (reviewed by Pugh and Lamb, 1993; Rieke and Baylor, 1998; Burns and Arshavsky, 2005); substantial differences in single photon responses indicate a previously unappreciated and surprising sensitivity of this process to experimental conditions. Second, comparison of signal and noise properties of rod responses with those inferred from behavioral measurements has shaped investigation of the retinal circuits dedicated to low light level vision; this work has revealed several signal processing mechanisms that appear near-ideally matched to properties of the single photon response (Bialek and Owen, 1990; Rieke and Baylor, 1996b; Field and Rieke, 2002; Armstrong-Gold and Rieke, 2003; Sampath and Rieke, 2004). These mechanisms, as well as other aspects of our understanding of retinal processing, will need to be reevaluated if they are based on non-physiological photoreceptor responses. Below we discuss our results in the context of these issues.

Cold L-15 medium accelerates the single rod responses and adversely affects the health of retinal tissue

Storing the retina in L-15, either warm or cold, had dramatic effects on both the responses of single rod photoreceptors and the general health of the retina. Responses of rods recorded in Locke's medium retained a dependence on how the retina was stored: cold L-15 storage resulted in smaller and faster single photon responses than other storage conditions, even when the same conditions were used during actual recordings. Assuming the transduction cascade operates linearly at low light levels, its kinetics are controlled by two factors - the rate of decay of light-activated PDE activity and the dark PDE activity level (Rieke and Baylor, 1996a). The dominant time constant for bright flashes, however, had at most a weak dependence on how the retina was stored. Assuming the same process dominates the rate of decay of PDE activity for bright and dim flashes, the weak dependence of the dominant time constant on storage conditions makes changes in the decay of PDE activity unlikely to explain the effect of L-15 on the single photon response. Instead our results are most consistent with an increased rate of dark PDE activity and corresponding speeding of the response of the transduction cascade to perturbations in cGMP concentration; simple

transduction cascade models would require a ~3-fold increase in dark PDE activity to account for the difference in kinetics between the responses from retina stored in Locke's vs cold L-15 (Nikonov et al., 2000).

While the rods appeared healthy and generated robust light responses in retina stored in L-15, the remainder of the retina showed clear morphological and physiological abnormalities. In particular, L-15 storage precluded comparing rod responses with those of downstream neurons. This effect of L-15 storage is consistent with observations by Ames and Nesbett (Ames and Nesbett, 1981) during their original formulation of Ames' medium: they noted that typical culture solutions did not preserve the morphology, metabolism, or light responsiveness of rabbit retina. Winkler et al. (1977) (Winkler et al., 1977) similarly found that the ERG b-wave disappeared following storage in solutions with phosphate or Tris pH buffering. Taken together, these studies suggest that bicarbonate, which is absent in L-15, is critical for maintaining normal retinal morphology and function.

The ERG a-wave is insensitive to alterations in rod phototransduction

The electroretinogram is often used to infer *in vivo* properties of the rod responses (Lyubarsky and Pugh, 1996; Pepperberg et al., 1997; Hetling and Pepperberg, 1999; Friedburg et al., 2001). Our results raise two cautions about the generality of such an approach. First, manipulations that produced clear changes in measured rod responses had surprisingly little effect on the responses derived from the ERG. In particular, dominant time constants from ERG-derived responses were insensitive to alterations in the Mg^{2+} concentration, unlike the dominant time constants measured from single rods. Previous *in vivo* and *in vitro* ERG measurements also suggest that the ERG a-wave may not be directly proportional to the rod photocurrent; specifically, voltage changes measured along the longitudinal axis of the outer segments in response to bright flashes show a transient component that is absent in the photocurrent and likely originates in the inner retina (Green and Kapousta-Bruneau, 1999). A similar effect may reduce the sensitivity of the ERG to alterations in the rod photocurrents. Alternatively, the suction procedure itself may alter rod photocurrents in such a way as to eliminate important components comprising the ERG, though we did not see a corresponding transient component in voltage clamp recordings from the rod soma (data not shown; see also Baylor and Nunn, 1986 (Baylor and Nunn, 1986)).

Second, paired-flash protocols used to derive rod responses to sub-saturating lights rely on the first flash producing a substantial suppression of current. Typically such measurements are made for initial flashes producing close to a half-maximal response (Pepperberg et al., 1997; Hetling and Pepperberg, 1999; Friedburg et al., 2001). When measured in single cells, however, the kinetics of half-maximal responses differ considerably from single photon responses (Baylor et al., 1979b). Consequently, derived sub-saturating flash responses from the ERG are not comparable with the rod's single photon response. Furthermore, half-maximal responses of single rods showed little dependence on recording conditions; the same was true for derived sub-saturating responses from the ERG. The striking difference in single photon responses and minimal difference in half-saturating responses across conditions could be at least partially explained if calcium feedback to the rate of cGMP synthesis operates strongly and nonlinearly for brighter flashes (Burns et al., 2002), leading to a shift in the time constants controlling changes in cGMP.

We hoped to use the rod responses derived from the ERG to identify *in vitro* conditions producing rod responses that replicated those *in vivo*. This did not prove possible because of the insensitivity of the *in vitro* ERGs to manipulations that produced substantial changes in single rod responses. In particular, the similarity of ERG-derived rod responses prevented us from identifying Mg^{2+} and Ca^{2+} concentrations required to replicate *in vivo* conditions.

Increases in divalent ions accelerate recovery kinetics in responses to bright flashes

Under some conditions, the dim flash response recovers with a time course similar to the dominant time constant for the decay of light-activated PDE activity. However, several manipulations cause the time constant of the recovery of the dim flash response to differ from the dominant time constant. For example, underexpression of rhodopsin kinase (GRK1) in recording solutions with high divalent concentrations produces a clear slowing of the dim flash response with little change in the dominant time constant (Chen et al., 2010). Similarly, lack of recoverin speeds the dim flash response with a less dramatic change in dominant time constant (Makino et al., 2004). Differences in responses at low and high Mg^{2+} concentrations provide a dramatic example: dim flash responses recovered ~10–15% more quickly at high Mg^{2+} while the dominant time constant was nearly 2-fold smaller (Fig. 5).

Changing the Mg^{2+} concentration also had unexpected effects on the response area (i.e. integrated response). If the measured transduction currents are linearly proportional to the light-activated PDE activity (Burns et al., 2002), then a 2-fold change in the dominant time constant should produce a 2-fold change in response area. Whether this change in area is produced by a change in response amplitude, kinetics or both will depend on the cGMP turnover rate and how closely the cGMP concentration tracks the PDE activity (Nikonov et al., 2000). Single photon response areas, however, showed a much weaker dependence on Mg^{2+} concentration than the dominant time constant. This indicates either that (1) the gain and/or time course of the PDE activity estimated from bright flashes fails to apply to dim flashes, or (2) changing Mg^{2+} has multiple effects, not all of which are captured by the dominant time constant. The rate of cGMP synthesis is known to depend on magnesium (Peshenko et al., 2008), but a simple scaling of the synthesis rate would equally affect the time in saturation at all flash strengths (Burns and Pugh, 2009), leaving the estimate of the dominant time constant unchanged. Instead, the sensitivity of τ_d to Mg^{2+} is unexpected, and it will be interesting to understand this effect in more mechanistic detail.

Importance for visual sensitivity

The behavioral performance of the visual system of many vertebrates approaches limits set by the division of light into discrete photons and noise in the responses of the rod photoreceptors (Hecht et al., 1942; Sakitt, 1972; Aho et al., 1988; Naarendorp et al., 2010). This observation has motivated considerable theoretical and experimental work to understand retinal processing at visual threshold. For example, absolute visual sensitivity places at least two requirements on the transmission of signals from rods to rod bipolar cells. First, the reduction in transmitter release produced during the hyperpolarizing single photon response must be distinguishable from synaptic noise (Rao-Mirotznik et al., 1998; Schein and Ahmad, 2005; Schein and Ahmad, 2006). Fluctuations in vesicle release in the dark will produce random pauses or slowing in release that could be confounded with true single photon responses. The effect of such synaptic noise on visual sensitivity will depend strongly on how much and for how long the single photon response suppresses the release rate, which in turn depends on the amplitude and kinetics of the single photon response. Second, transmission from rods to rod bipolar cells must separate single photon responses in a minority of the converging rods inputs from continuous noise generated in the majority (Baylor et al., 1984; van Rossum and Smith, 1998). A thresholding nonlinearity at the rod-to-rod bipolar synapse appears to serve such a role (Field and Rieke, 2002; Sampath and Rieke, 2004). The effectiveness of such a mechanism has a strong dependence on how well it is matched to the signal and noise properties of the rod responses (Okawa et al., 2010). Thus the effect of experimental conditions on the single photon response amplitude and kinetics is important for our understanding of the operation both of phototransduction and of downstream processes critical in preserving the fidelity of rod vision.

Acknowledgments

We are grateful to Clint Makino for the detailed protocol for experiments using L-15 and Locke's solutions; Jon Cafaro, Peter Detwiler, Thuy Doan, Greg Field, Jim Hurley, and Alapakkam Sampath for critical reading of the manuscript; the Rieke and Perkel lab members for many helpful discussions; Paul Newman, Richard Ahlquist, and Eric Martinson for excellent technical support. Support was provided by the NIH through grants EY-11850 (F.R.), T32GM-07270 (A.W.A), and the Howard Hughes Medical Institute (F.R.).

References

Aho AC, Donner K, Hyden C, Larsen LO, Reuter T. Low retinal noise in animals with low body temperature allows high visual sensitivity. Nature. 1988; 334:348–350. [PubMed: 3134619]

Ames, Ar; Nesbett, FB. In vitro retina as an experimental model of the central nervous system. J Neurochem. 1981; 37:867–877. [PubMed: 7320727]

Armstrong-Gold CE, Rieke F. Bandpass filtering at the rod to second-order cell synapse in salamander (Ambystoma tigrinum) retina. J Neurosci. 2003; 23:3796–3806. [PubMed: 12736350]

Baylor DA, Hodgkin AL. Detection and resolution of visual stimuli by turtle photoreceptors. J Physiol. 1973; 234:163–198. [PubMed: 4766219]

Baylor DA, Lamb TD, Yau KW. Responses of retinal rods to single photons. J Physiol. 1979a; 288:613–634. [PubMed: 112243]

Baylor DA, Lamb TD, Yau KW. The membrane current of single rod outer segments. J Physiol. 1979b; 288:589–611. [PubMed: 112242]

Baylor DA, Nunn BJ. Electrical properties of the light-sensitive conductance of rods of the salamander Ambystoma tigrinum. J Physiol. 1986; 371:115–145. [PubMed: 2422346]

Baylor DA, Nunn BJ, Schnapf JL. The photocurrent, noise and spectral sensitivity of rods of the monkey Macaca fascicularis. J Physiol. 1984; 357:575–607. [PubMed: 6512705]

Bialek W, Owen WG. Temporal filtering in retinal bipolar cells. Elements of an optimal computation? Biophys J. 1990; 58:1227–1233. [PubMed: 2291942]

Burns ME, Arshavsky VY. Beyond Counting Photons: Trials and Trends in Vertebrate Visual Transduction. Neuron. 2005; 48:387–401. [PubMed: 16269358]

Burns ME, Mendez A, Chen J, Baylor DA. Dynamics of cyclic GMP synthesis in retinal rods. Neuron. 2002; 36:81–91. [PubMed: 12367508]

Burns ME, Pugh ENJ. RGS9 concentration matters in rod phototransduction. Biophys J. 2009; 97:1538–1547. [PubMed: 19751658]

Burns ME, Pugh ENJ. Lessons from photoreceptors: turning off g-protein signaling in living cells. Physiology (Bethesda). 2010; 25:72–84. [PubMed: 20430952]

Calvert PD, Govardovskii VI, Krasnoperova N, Anderson RE, Lem J, Makino CL. Memebrane protein diffusion sets the speed of rod phototransduction. Nature. 2001; 411

Calvert PD, Krasnoperova NV, Lyubarsky AL, Isayama T, Nicolo M, Kosaras B, Wong G, Gannon KS, Margolskee RF, Sidman RL, Pugh ENJ, Makino CL, Lem J. Phototransduction in transgenic mice after targeted deletion of the rod transducin alpha -subunit. Proc Natl Acad Sci U S A. 2000; 97:13913–13918. [PubMed: 11095744]

Chen CK, Burns ME, He W, Wensel TG, Baylor DA, Simon MI. Slowed recovery of rod photoresponse in mice lacking the GTPase accelerating protein RGS9-1. Nature. 2000; 403:557–560. [PubMed: 10676965]

Chen CK, Woodruff ML, Chen FS, Chen D, Fain GL. Background light produces a recoverin-dependent modulation of activated-rhodopsin lifetime in mouse rods. J Neurosci. 2010; 30:1213–1220. [PubMed: 20107049]

Davenport CM, Detwiler PB, Dacey DM. Effects of pH buffering on horizontal and ganglion cell light responses in primate retina: evidence for the proton hypothesis of surround formation. J Neurosci. 2008; 28:456–464. [PubMed: 18184788]

Doan T, Azevedo AW, Hurley JB, Rieke F. Arrestin competition influences the kinetics and variability of the single-photon responses of mammalian rod photoreceptors. J Neurosci. 2009; 29:11867–11879. [PubMed: 19776273]

Doan T, Mendez A, Detwiler PB, Chen J, Rieke F. Multiple phosphorylation sites confer reproducibility of the rod's single-photon responses. Science. 2006; 313:530–533. [PubMed: 16873665]

Fahrenfort I, Steijaert M, Sjoerdsma T, Vickers E, Ripps H, van Asselt J, Endeman D, Klooster J, Numan R, ten Eikelder H, von Gersdorff H, Kamermans M. Hemichannel-mediated and pH-based feedback from horizontal cells to cones in the vertebrate retina. PLoS ONE. 2009; 4:e6090. [PubMed: 19564917]

Field GD, Rieke F. Nonlinear signal transfer from mouse rods to bipolar cells and implications for visual sensitivity. Neuron. 2002; 34:773–785. [PubMed: 12062023]

Field GD, Sampath AP, Rieke F. Retinal processing near absolute threshold: from behavior to mechanism. Annu Rev Physiol. 2005; 67:491–514. [PubMed: 15709967]

Friedburg C, Thomas MM, Lamb TD. Time course of the flash response of dark- and light-adapted human rod photoreceptors derived from the electroretinogram. J Physiol. 2001; 534:217–242. [PubMed: 11433004]

Fu Y, Kefalov V, Luo DG, Xue T, Yau KW. Quantal noise from human red cone pigment. Nat Neurosci. 2008; 11:565–571. [PubMed: 18425122]

Green DG, Kapousta-Bruneau NV. A dissection of the electroretinogram from the isolated rat retina with microelectrodes and drugs. Vis Neurosci. 1999; 16:727–741. [PubMed: 10431921]

Gross OP, Burns ME. Control of rhodopsin's active lifetime by arrestin-1 expression in mammalian rods. J Neurosci. 2010; 30:3450–3457. [PubMed: 20203204]

Hecht S, Shlaer S, Pirenne MH. Energy, quanta, and vision. J Gen Physiol. 1942; 25:819–840. [PubMed: 19873316]

Herrmann R, Lobanova ES, Hammond T, Kessler C, Burns ME, Frishman LJ, Arshavsky VY. Phosducin regulates transmission at the photoreceptor-to-ON-bipolar cell synapse. J Neurosci. 2010; 30:3239–3253. [PubMed: 20203183]

Hetling JR, Pepperberg DR. Sensitivity and kinetics of mouse rod flash responses derived in vivo from paired-flash electroretinograms. J Physiol. 1999; 516:593–609. [PubMed: 10087356]

Hirasawa H, Kaneko A. pH changes in the invaginating synaptic cleft mediate feedback from horizontal cells to cone photoreceptors by modulating Ca2+ channels. J Gen Physiol. 2003; 122:657–671. [PubMed: 14610018]

Krispel CM, Chen D, Melling N, Chen YJ, Martemyanov KA, Quillinan N, Arshavsky VY, Wensel TG, Chen CK, Burns ME. RGS expression rate-limits recovery of rod photoresponses. Neuron. 2006; 51:409–416. [PubMed: 16908407]

Luo DG, Yau KW. Rod sensitivity of neonatal mouse and rat. J Gen Physiol. 2005; 126:263–269. [PubMed: 16129773]

Lyubarsky AL, Pugh J, Edward N. Recovery phase of the murine rod photoresponse reconstructed from electroretinographic recordings. J Neurosci. 1996; 16:563–571. [PubMed: 8551340]

Makino CL, Dodd RL, Chen J, Burns ME, Roca A, Simon MI, Baylor DA. Recoverin regulates light-dependent phosphodiesterase activity in retinal rods. J Gen Physiol. 2004; 123:729–741. [PubMed: 15173221]

Mendez A, Burns ME, Sokal I, Dizhoor AM, Baehr W, Palczewski K, Baylor DA, Chen J. Role of guanylate cyclase-activating proteins (GCAPs) in setting the flash sensitivity of rod photoreceptors. Proc Natl Acad Sci U S A. 2001; 98:9948–9953. [PubMed: 11493703]

Mendez A, Burns ME, Roca A, Lem J, Wu L-W, Simon MI, Baylor DA, Chen J. Rapid and reproducible deactivation of rhodopsin requires multiple phosphorylation sites. Neuron. 2000; 28:153–164. [PubMed: 11086991]

Naarendorp F, Esdaille TM, Banden SM, Andrews-Labenski J, Gross OP, Pugh ENJ. Dark light, rod saturation, and the absolute and incremental sensitivity of mouse cone vision. J Neurosci. 2010; 30:12495–12507. [PubMed: 20844144]

Nikonov S, Lamb TD, Pugh ENJ. The role of steady phosphodiesterase activity in the kinetics and sensitivity of the light-adapted salamander rod photoresponse. J Gen Physiol. 2000; 116:795–824. [PubMed: 11099349]

Okawa H, Miyagishima KJ, Arman AC, Hurley JB, Field GD, Sampath AP. Optimal processing of photoreceptor signals is required to maximize behavioural sensitivity. J Physiol. 2010; 588:1947–1960. [PubMed: 20403975]

Pepperberg D, Cornwall M, Kahlert M, Hofmann K, Jin J, Jones G, Ripps H. Light-dependent delay in the falling phase of the retinal rod photoresponse. Visual Neuroscience. 1992; 8:9–18. [PubMed: 1739680]

Pepperberg DR, Birch DG, Hood DC. Photoresponses of human rods in vivo derived from paired-flash electroretinograms. Vis Neurosci. 1997; 14:73–82. [PubMed: 9057270]

Peshenko IV, Olshevskaya EV, Dizhoor AM. Binding of guanylyl cyclase activating protein 1 (GCAP1) to retinal guanylyl cyclase (RetGC1). The role of individual EF-hands. J Biol Chem. 2008; 283:21747–21757. [PubMed: 18541533]

Pugh ENJ, Lamb TD. Amplification and kinetics of the activation steps in phototransduction. Biochim Biophys Acta. 1993; 1141:111–149. [PubMed: 8382952]

Rao-Mirotznik R, Buchsbaum G, Sterling P. Transmitter concentration at a three-dimensional synapse. J Neurophysiol. 1998; 80:3163–3172. [PubMed: 9862914]

Rieke F, Baylor DA. Molecular origin of continuous dark noise in rod photoreceptors. Biophys J. 1996a; 71:2553–2572. [PubMed: 8913594]

Rieke F, Baylor DA. Postsynaptic calcium feedback between rods and rod bipolar cells in the mouse retina. Biophys J. 1996b; 71:913–924.

Rieke F, Baylor DA. Single-photon detection by rod cells of the retina. Reviews of Modern Physics. 1998; 70:1027–1036.

Robson JG, Maeda H, Saszik SM, Frishman LJ. In vivo studies of signaling in rod pathways of the mouse using the electroretinogram. Vision Res. 2004; 44:3253–3268. [PubMed: 15535993]

Sakitt B. Counting every quantum. J Physiol. 1972; 223:131–150. [PubMed: 5046137]

Sampath AP, Rieke F. Selective transmission of single photon responses by saturation at the rod-to-rod bipolar synapse. Neuron. 2004; 41:431–443. [PubMed: 14766181]

Sampath AP, Strissel KJ, Elias R, Arshavsky VY, McGinnis JF, Chen J, Kawamura S, Rieke F, Hurley JB. Recoverin improves rod-mediated vision by enhancing signal transmission in the mouse retina. Neuron. 2005; 46:413–420. [PubMed: 15882641]

Saszik SM, Robson JG, Frishman LJ. The scotopic threshold response of the dark-adapted electroretinogram of the mouse. J Physiol. 2002; 543:899–916. [PubMed: 12231647]

Schein S, Ahmad KM. A clockwork hypothesis: synaptic release by rod photoreceptors must be regular. Biophys J. 2005; 89:3931–3949. [PubMed: 16169984]

Schein S, Ahmad KM. Efficiency of synaptic transmission of single-photon events from rod photoreceptor to rod bipolar dendrite. Biophys J. 2006; 91:3257–3267. [PubMed: 16920838]

Schnapf JL, Nunn BJ, Meister M, Baylor DA. Visual transduction in cones of the monkey Macaca fascicularis. J Physiol. 1990; 427:681–713. [PubMed: 2100987]

Sharpe LT, Stockman II. Rod pathways: the importance of seeing nothing, by Lindsay T. Sharpe and Andrew Stockman, Vol. 22, pp 497–504. Trends Neurosci. 2000; 23:39. [PubMed: 10637644]

van Rossum MC, Smith RG. Noise removal at the rod synapse of mammalian retina. Vis Neurosci. 1998; 15:809–821. [PubMed: 9764523]

Wen XH, Shen L, Brush RS, Michaud N, Al-Ubaidi MR, Gurevich VV, Hamm HE, Lem J, Dibenedetto E, Anderson RE, Makino CL. Overexpression of rhodopsin alters the structure and photoresponse of rod photoreceptors. Biophys J. 2009; 96:939–950. [PubMed: 19186132]

Winkler BS, Simson V, Benner J. Importance of bicarbonate in retinal function. Invest Ophthalmol Vis Sci. 1977; 16:766–768. [PubMed: 885685]

Xu J, Dodd RL, Makino CL, Simon MI, Baylor DA, Chen J. Prolonged photoresponses in transgenic mouse rods lacking arrestin. Nature. 1997; 389:505–509. [PubMed: 9333241]

Yau KW, Lamb TD, Baylor DA. Light-induced fluctuations in membrane current of single toad rod outer segments. Nature. 1977; 269:78–80. [PubMed: 408711]

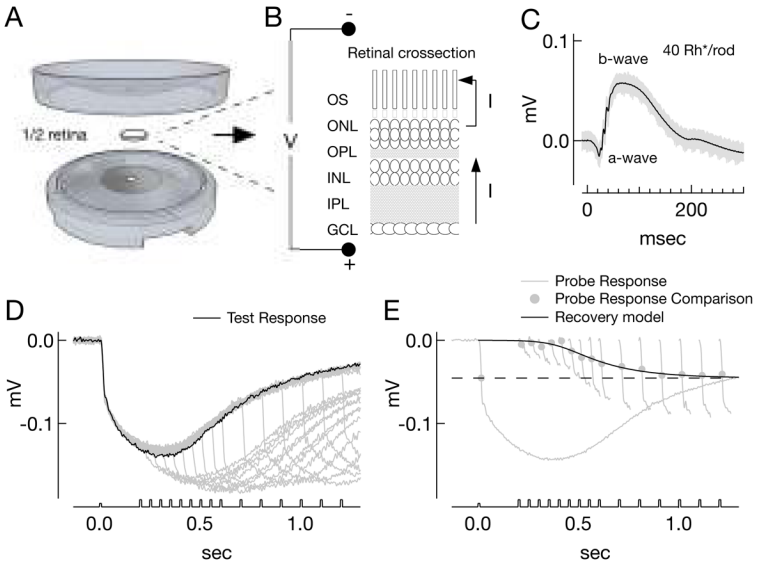

Figure 1. ERG methods and description of paired-pulse derivation of rod responses

A) ERG recording apparatus, scale is approximate. The space between top and bottom where the retina was placed measured ~12mm in diameter and 300μm high. B) Schematic cross-section of retina and measurement of the ERG (OS -photoreceptor outer segments; ONL - outer nuclear layer; OPL - outer plexiform layer; INL - inner nuclear layer; IPL - inner plexiform layer; GCL - ganglion cell layer). C) Twenty raw ERGs (grey) and average (black) following a 0.2ms flash producing 40Rh*/rod in Ames'/Ames' conditions. Reduction in current flowing along the photoreceptor outer segments in response to light results in the corneal-negative deflection of the ERG termed the a-wave, while the b-wave reflects responses of second-order neurons. D–E) Paired-pulse analysis to derive rod responses in Ames'/Ames', with 4mM Aspartate which eliminates the b-wave (see Methods). D) Overlaid responses (grey traces) to paired test (840Rh*/rod) and probe flashes (1680Rh*/rod) presented at increasing intervals; the response to the test flash alone is shown in black. E) The probe response rising phases from (D) (short traces, baseline corrected) are compared to the response to the probe flash alone (complete trace). Comparison is made at the time point of fastest rate of change of the response to the probe alone (dot, black dashed line). The ratio of the rising phase amplitude at this point, to the amplitude of the probe alone response (dashed black line) maps out a derived rod response. The recovery points are then fit with a model recovery function ($F'(t) = \{1+\exp[a(t-t_{1/2})]\}^{-h}$, $t_{1/2}$ = 405 ms, a = 14.4, h = 0.3). For illustration purposes in this panel, the black trace plots the function, $p\ [1-F'(t)]$, where $p = -45\mu V$ is the amplitude of the response to the probe alone (dashed black line).

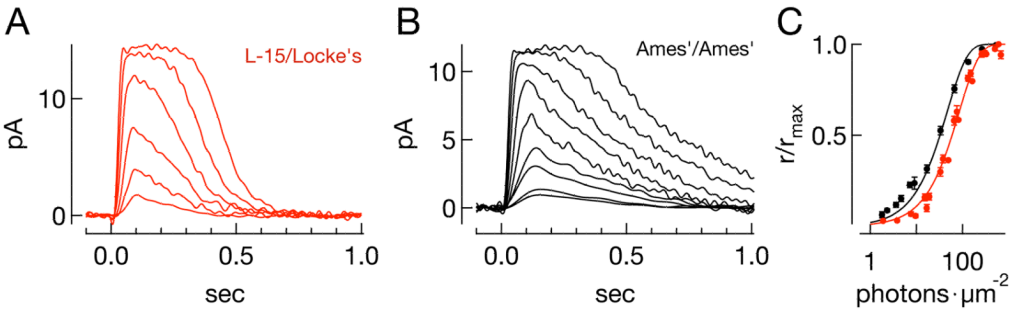

Figure 2. Rod sensitivity depends on the experimental protocol

A–B) Family of flash responses from a rod in (A) L-15/Locke's and in (B) Ames'/Ames' conditions. Flash strengths double over ranges of (A) 17–524 and (B) 2–516photons μm^{-2}. C) The peak fractional current suppression (r/r_{max}) as a function of the flash strength (mean ± SEM, n=19 for Ames'/Ames' and 15 for L15/Locke's). Smooth curves are the saturating exponentials that best fit the population data, with I_0 = 57photons μm^{-2} for L-15/Locke's (red), and 28photons μm^{-2} for Ames'/Ames' (black).

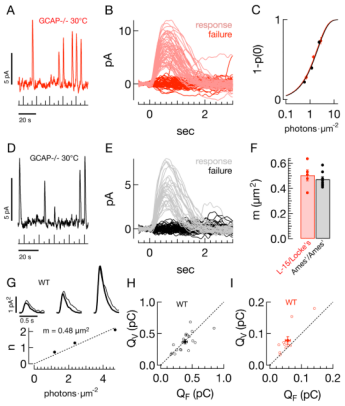

Figure 3. The rod collecting area does not depend on the experimental protocol

A–F) Frequency of seeing analysis for GCAP$^{-/-}$ rods. A) Raw current trace from GCAP$^{-/-}$ rod in L-15/Locke's, showing responses to three repeated flash strengths (0.7, 1.4, 2.8photons μm^{-2}, stimulus trace below, 30°C). B) Superimposed responses to a flash with strength of 1.4photons μm^{-2}, p(0) = 0.54. C) The average probability of observing a response (1-p(0)), as a function of flash strength, for populations of GCAP$^{-/-}$ rods in both L-15/Locke's (red, n=5) and Ames'/Ames' (black, n=8). Smooth lines show the Poisson prediction, $1-p_0(I) = 1-e^{-mI}$, with m = 0.50μm^2 in L-15/Locke's and 0.47μm^2 in Ames'/Ames'. D) Raw current trace for Ames'/Ames' condition (flash strengths: 0.6, 1.2, 2.4photons μm^{-2}). E) Superimposed responses to a flash with strength of 1.2photons μm^{-2}, p(0) = 0.64. F) Collecting areas (CA) from individual GCAP$^{-/-}$ rods in L-15/Locke's (red, 0.50 ± 0.04μm^2), and Ames'/Ames' (black, 0.47 ± 0.02μm^2). G–I) Comparison of variance and frequency of seeing estimates. G) (top) Variance (thin trace) and scaled mean-squared response (thick trace) in a representative rod in Ames'/Ames' (see Methods) for flash strengths of 1.18, 2.36, and 4.72photons μm^{-2}. Scale bars are 0.5sec and 1pA^2. The reciprocal of the scale factor applied to the mean-squared response gives the mean number of effective photon absorptions, *n*. (bottom) The collecting area, *m*, is the slope of the best fit line (dotted line) through the *n* vs *I* data, in this case 0.48μm^2. H) Population data in Ames'/Ames' for the integral of the estimated single photon response using the variance-to-mean-squared method, Q_V (y-axis, pC) and using a fixed collecting area of 0.5μm^2, Q_F (x-axis, pC). Filled circles give the average across the population ± SEM. I) Same as (H) for L-15/Locke's.

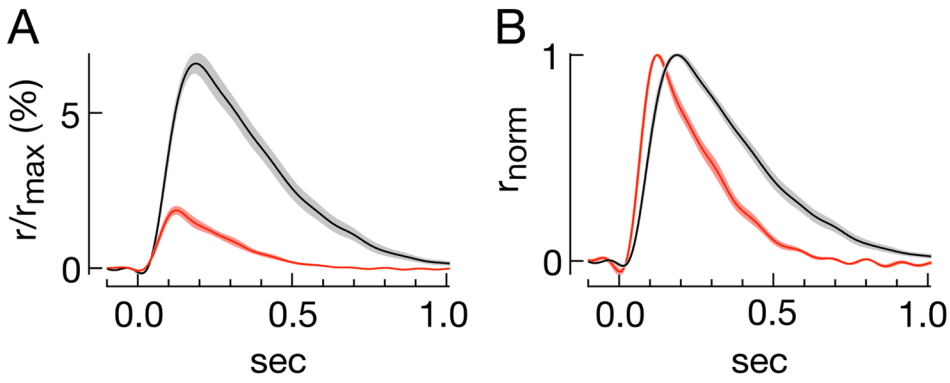

Figure 4. The single photon response depends on the experimental protocol

A) Average single photon responses as a percentage of suppressible current for rods in L-15/Lockes (red, n=15) and Ames'/Ames' (black, n=20). Contours are the SEM across a population of rods. B) Normalized responses from (A).

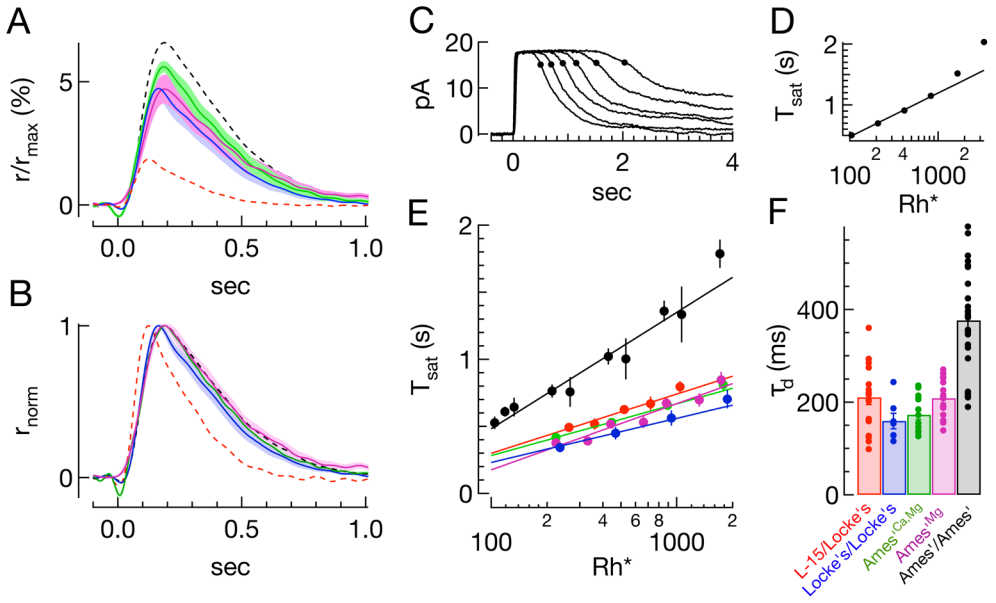

Figure 5. Dependence of single photon response and dominant time constant of recovery on divalent concentration

A) Average single photon responses in different conditions (±SEM), using a fixed collecting area: Locke's/Locke's (blue), Ames'^{Ca,Mg}/Ames'^{Ca,Mg} (green), and Ames'^{Mg}/Ames'^{Mg} (magenta). The Ames' conditions match either Mg^{2+} alone or both Ca^{2+} and Mg^{2+} concentrations in Locke's. B) Normalized single photon responses in the same conditions and colors. Dashed lines in (A) and (B) show single photon responses from Figure 4: L-15/Locke's (red), Ames'/Ames' (black). C–F) Estimate of the dominant time constant for recovery of light-activated PDE activity. C–D) Illustration of the technique: For a family of responses to bright flashes (Ames'/Ames'; 105, 208, 415, 829, 1658, 3315Rh*), the time at which a response recovers 15% of the dark current (C) is plotted against the logarithm of the flash strength (D). The slope of this linear relationship estimates the dominant time constant of recovery, in this case 312ms. E) Average (log(i), T_{sat}) pairs for all cells in a given condition; only points below 1000 Rh* are fit. Slopes of best fit lines are as follows: L-15/Locke's - 192ms; Locke's/Locke's - 143ms; Ames'^{Ca,Mg}/Ames'^{Ca,Mg} - 168ms; Ames'^{Mg}/Ames'^{Mg} - 214ms; Ames'/Ames' - 371ms. F) Summary of dominant time constants from fits to data from individual rods as in D (see also Table 1).

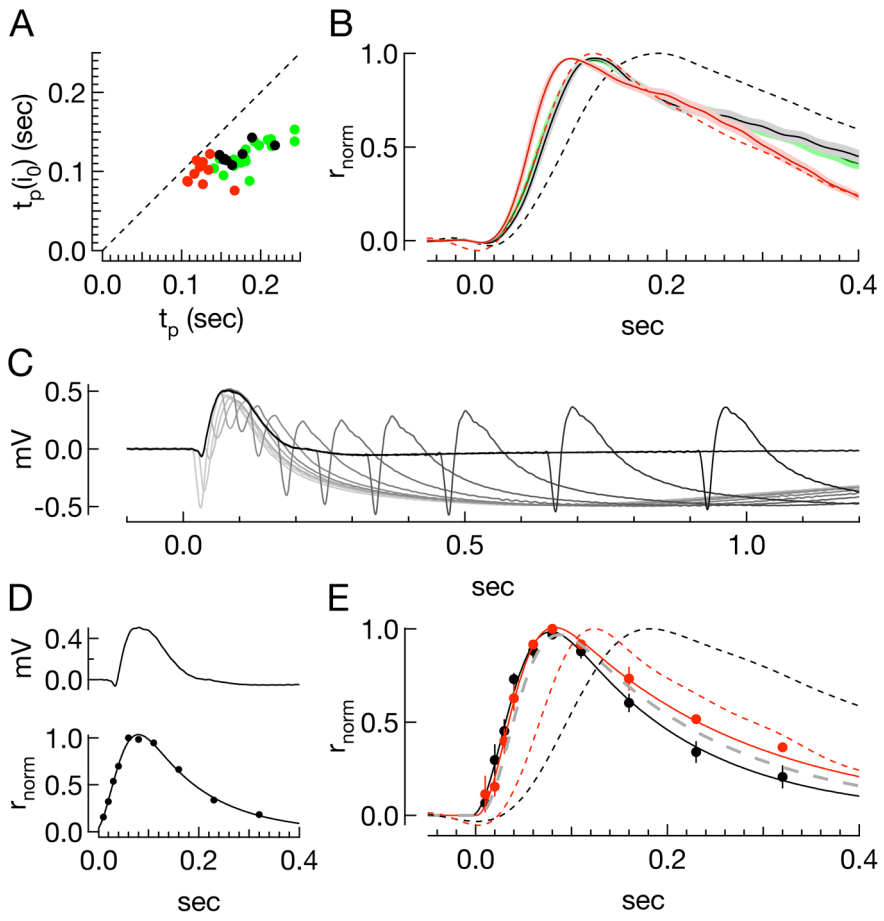

Figure 6. Dominant time constants of ERG-derived rod responses show little dependence on divalent concentration

A) ERGs in response to increasing delays between a test (834Rh*) and probe (834Rh*) flash (stimulus trace below). Black responses are followed through the subsequent panels. B) Rising phases of the responses to the probe flash, aligned to the time of the flash, when presented alone (thick black trace), and when following a test flash. Dots represent points of comparison to the thick curve, at the point of fastest change (18ms). This comparison measures the fraction of the remaining rod response, $R(t_i)$. C) Fractional response suppression, $F(t_i) = 1-R(t_i)$, as a function of the delay between test and probe flashes; the smooth gray curve is the best fit recovery function (see Methods, $t_{1/2}$ = 210 ms, a = 30.6, h = 0.1). The thin black trace is the ERG in response to the test flash alone. Inset: four derived rod responses (298, 417, 596, 834Rh*). The dashed line plots the 50% criterion level used to determine the dominant time constant. D) Paired-pulse analysis in single rod outer segments (664 Rh*; inset: 332, 664, 1327Rh*). E) Comparison of dominant time constants for ERG-derived responses in Ames'/Ames' (n=9) and Ames'^{Ca,Mg}/Ames'^{Ca,Mg} (n=5) conditions and single rod recordings using paired-pulse analysis or directly from the current response (as in Fig. 5). Lines for single cell recordings connect measures from the same cell.

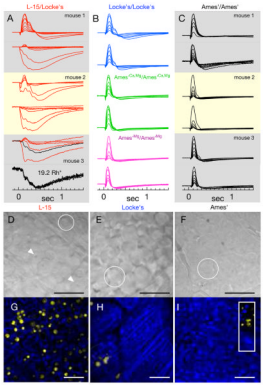

Figure 7. Single rod and ERG-derived responses to half-saturating flashes exhibit similar kinetics across conditions

A) The time-to-peak of the half-saturating response (y-axis) for single rod recordings plotted against time-to-peak of the single photon response (x-axis). B) Population mean normalized half-saturating outer segment current responses in L-15/Locke's, Ames'^{Ca,Mg}/Ames'^{Ca,Mg}, and Ames'/Ames', and the normalized single photon response in L-15/Locke's and Ames'/Ames' (red and black dashed lines, see Fig. 4). C) ERGs in response to increasing delays between test (27Rh*) and probe (2400Rh*) flashes. D) Isolated ERG response to a flash producing 27Rh* in Ames' and the normalized derived rod response using the paired-pulse technique to the same test flash strength. Smooth curve fit to the data is $r(t) = \gamma[(1-\exp(-\alpha(t-t_d)^2)]\exp(-1/\tau)$, $t_d = -7.8$ms, $\gamma = 2.4$, $\alpha = 2.3\times10^{-4}$ms^2, $\tau_\omega = 121$ms. E) Average derived rod responses in Ames'/Ames' (black, $t_d = -4.1$ms, $\gamma = 1.7$, $\alpha = 3.0\times10^{-4}$ms^2, $\tau_\omega = 134$ms) and L-15/Locke's (red, $t_d = 0.56$ms, $\gamma = 1.7$, $\alpha = 3.8\times10^{-4}$ms^2, $\tau_\omega = 191$ms). The grey dashed line is the same model using the *in vivo* ERG-derived parameters {Hetling 1999}, ($t_d = 3.1$ms, $\gamma = 1.84$, $\alpha = 3.23\times10^{-4}$ms^2, $\tau_\omega = 163$ms). The dashed lines plots the normalized single photon response in L-15/Locke's and Ames'/Ames' (red and black dashed lines, see Fig. 4).

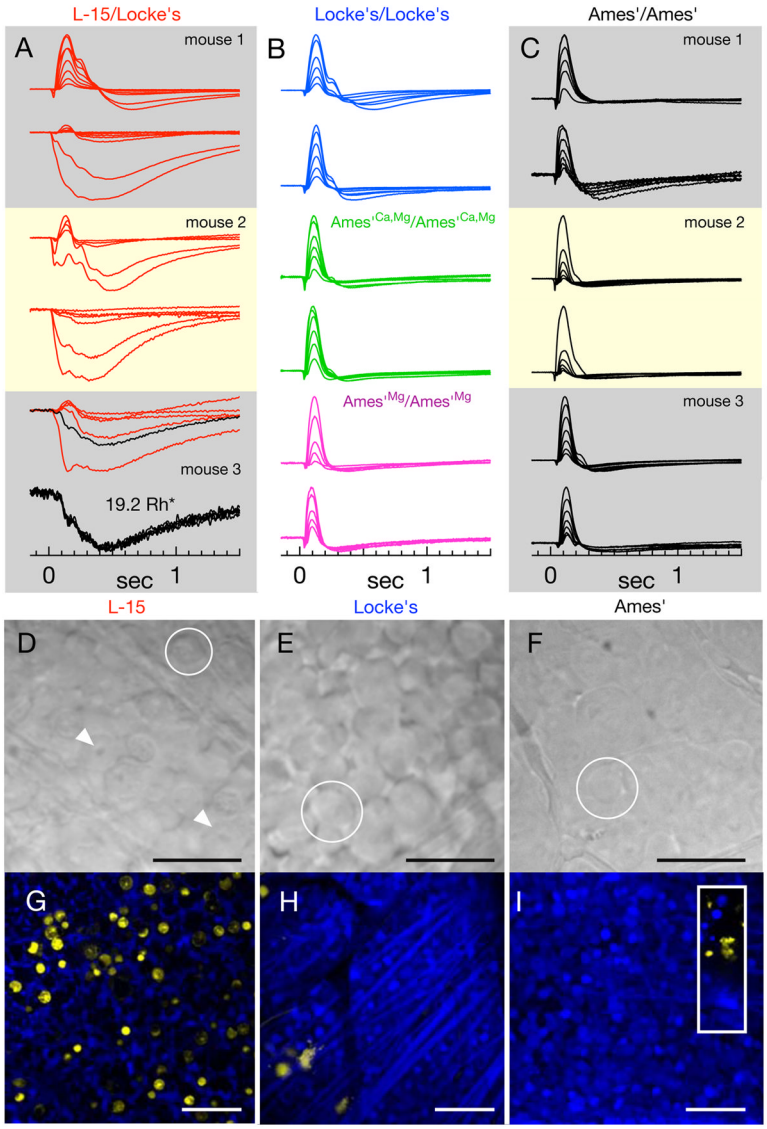

Figure 8. The viability of retinal tissue under different conditions: *in vitro* ERGs, morphology, Live/Dead staining

A–C) Normalized ERGs in response to flash families from individual isolated retinas (~0.5–40Rh*/rod). ERGs measured from half of one retina placed in L-15/Locke's conditions (A, both halves in one box) were followed by ERG recordings from the other retina in Ames'/Ames' (C, labels identify retina from the same mouse). Each trace is the average of ~5 responses. The bottom panel depicts individual responses comprising the trace in black in the above flash family (19.2Rh*). B) Representative ERG families from tissue in Locke's/Locke's (blue), Ames'^{Ca,Mg}/Ames'^{Ca,Mg} (green), and Ames'^{Mg}/Ames'^{Mg} (magenta). ERGs of retina in L-15/Locke's exhibit greater variability than other conditions. D–F) DIC images of flat-mounted retinal tissue following storage in (D) cold L-15, (E) warm (32°C) Locke's medium, and (F) warm (32°C) Ames medium. Scale bars are 25μm. Circles indicate ganglion cell somas and arrows in (D) illustrate prominent, pockmarked nuclei. (G–I) Confocal images through the ganglion cell layer of live (blue) and dead (yellow) tissue following storage in (G) cold L-15, (H) warm Locke's, (I) Ames' (inset: yellow stained cells at the edge of the retina piece). Scale bars are 50μm. Counts of yellow nuclei (mean ± SEM)

in images of retina stored in: cold L-15 - 119±32 (n=8); warm Locke's - 5±1.7 (n=4); Ames' with elevated Mg^{2+} - 2 (n=2); Ames' - 2.6±0.9 (n=5). An image of healthy retina on this scale contained 286±16 ganglion cells.

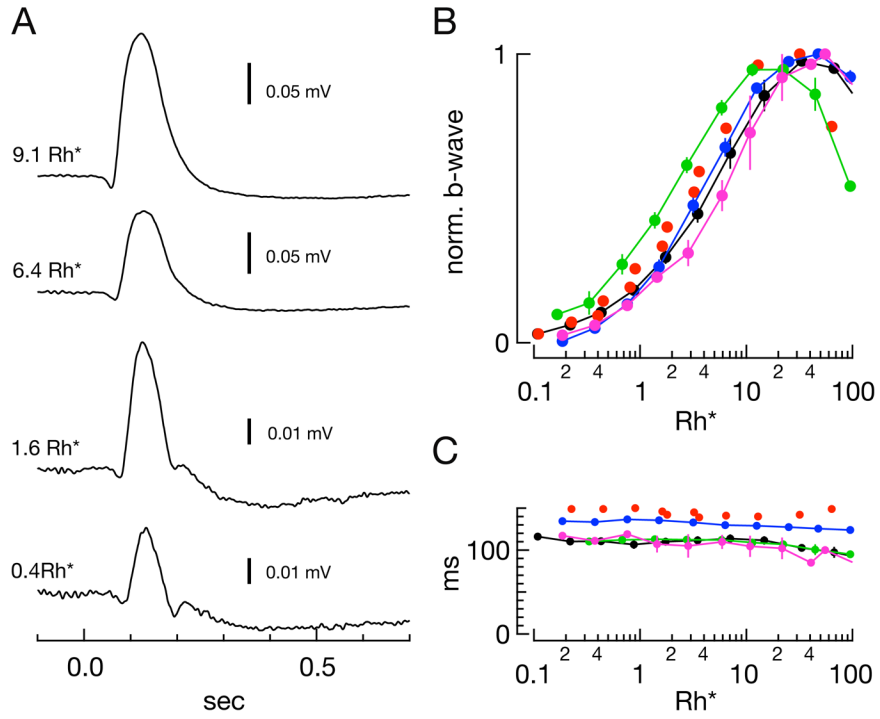

Figure 9. Properties of the *in vitro* scotopic ERG

A) Example Ames'/Ames' ERG traces at various flash strengths. B) Sensitivity of the b-wave amplitude across conditions for samples shown in Figure 8. Average half-saturating strengths in Rh*/rod: Locke's/Locke's (blue) - 3.2 Rh*/rod; Ames'/Ames' (black) - 4.0 Rh*/rod; Ames'^{Ca,Mg}/Ames'^{Ca,Mg} (green) - 1.8 Rh*/rod; Ames'$^{Mg/}$Ames'^{Mg} (magenta) - 5.7 Rh*/rod. Red dots in (B) and (C) represent the b-wave amplitudes of the one sample recorded in L-15/Locke's that exhibited a b-wave (Fig. 8H, top family). Half-saturating flash strength for this sample was 2.8 Rh*/rod. C) Average time-to-peak of the b-wave across conditions and flash strength for samples shown in Figure 8.

Table 1

Experimental Protocols, Shorthand Definitions

The designation denotes storage and perfusion solutions in each protocol. The color scheme defined here is held constant throughout the figures.

Designation	Color	Storage	Perfusion	Electrode
L-15/Locke's	Red	L-15 culture media on ice	Locke's, 36° C	HEPES Locke's, 36° C
Locke's/Locke's	Blue	Locke's, 32° C	Locke's, 36° C	HEPES Locke's, 36° C
Ames'/Ames'	Black	Bicarb. Ames, 32° C 1.15mM Ca^{2+}, 1.2 mM Mg^{2+}	Bicarb. Ames, 36° C 1.15mM Ca^{2+}, 1.2 mM Mg^{2+}	HEPES Ames, 36° C 1.15mM Ca^{2+}, 1.2 mM Mg^{2+}
Ames'^{Ca,Mg}/Ames'^{Ca,Mg}	Green	Bicarb. Ames, 32° C 1.2mM Ca^{2+}, 2.4 mM Mg^{2+}	Bicarb. Ames, 36° C 1.2mM Ca^{2+}, 2.4 mM Mg^{2+}	HEPES Ames, 36° C 1.2mM Ca^{2+}, 2.4 mM Mg^{2+}
Ames'^{Mg}/Ames'^{Mg}	Magenta	Bicarb. Ames, 32° C 2.4 mM Mg^{2+}	Bicarb. Ames, 36° C2.4 mM Mg^{2+}	HEPES Ames, 36° C 2.4 mM Mg^{2+}

Table 2

Summary Data from Single Rod Measurements

First five columns summarize properties of responses to dim flashes - peak: peak amplitude of the estimated single photon responses using a fixed collecting area of 0.5μm^2; t_p: time-to-peak of single photon response; t_i: integration time or area under the normalized single photon response; τ_r: exponential constant describing single photon response recovery phase. Dark current, r_{max}, is calculated from saturated responses. i_0 is the strength of the flash producing a half-maximal response, and $t_p(i_0)$ is the time-to-peak of that response. τ_d is the dominant time constant for decay of light-activated PDE activity (see Fig. 5).

Protocol	peak (pA)	t_p (ms)	t_i (ms)	τ_r (ms)	r_{max} (pA)	i_0 (photons μm^{-2})	t_p (i_0) (ms)	τ_D (ms)
L-15/Locke's	0.24 ± 0.03 (12)	127 ± 5	240 ± 11	174 ± 8	11.3 ± 0.5 (30)	57.4 ± 2.3 (15)	103 ± 4	210 ± 16 (21)
Warm L-15/Locke's	0.56 ± 0.08 (15)	159 ± 8	292 ± 25	217 ± 19	13.5 ± 0.9 (10)	-	-	-
Locke's/Locke's	0.82 ± 0.09 (13)	161 ± 5	324 ± 22	235 ± 19	16.9 ± 0.8 (22)	39.0 ± 1.8 (15)	124 ± 1	159 ± 17 (7)
Ames'/Ames'	1.04 ± 0.06 (19)	181 ± 6	369 ± 18	265 ± 17	15.1 ± 0.6 (50)	32.6 ± 2.2 (19)	127 ± 4	376 ± 23 (23)
Ames'^{Ca,Mg}/Ames'^{Ca,Mg}	0.90 ± 0.10 (20)	187 ± 6	332 ± 24	230 ± 22	14.5 ± 0.7 (29)	34.4 ± 1.6 (23)	125 ± 3	173 ± 10 (15)
Ames'^{Mg}/Ames'^{Mg}	0.60 ± 0.05 (30)	190 ± 5	318 ± 13	217 ± 10	13.5 ± 0.5 (33)	33.8 ± 3.5 (23)	124 ± 7	209 ± 10 (16)